HHS Public Access

Author manuscript

Pediatr Radiol. Author manuscript; available in PMC 2020 March 01.

Published in final edited form as:

Pediatr Radiol. 2019 March ; 49(3): 308–317. doi:10.1007/s00247-018-4312-8.

4-D flow MRI-derived energetic biomarkers are abnormal in children with repaired tetralogy of Fallot and associated with disease severity

Joshua D. Robinson[1,2,3], **Michael J. Rose**[4], **Maria Joh**[2,3], **Kelly Jarvis**[3,5], **Susanne Schnell**[3], **Alex J. Barker**[6], **Cynthia K. Rigsby**[2,3,4], and **Michael Markl**[3,5]

[1]Division of Pediatric Cardiology, Ann & Robert H. Lurie Children's Hospital of Chicago, 225 E. Chicago Ave., Box 21, Chicago, IL 60611, USA

[2]Department of Pediatrics, Ann & Robert H. Lurie Children's Hospital of Chicago, Chicago, IL, USA

[3]Department of Radiology, Feinberg School of Medicine, Northwestern University, Chicago, IL, USA

[4]Department of Medical Imaging, Ann & Robert H. Lurie Children's Hospital of Chicago, Chicago, IL, USA

[5]Department of Biomedical Engineering, McCormick School of Engineering, Northwestern University, Chicago, IL, USA

[6]Department of Radiology, University of Colorado, Aurora, CO, USA

Abstract

Background—Cardiac MRI plays a central role in monitoring children with repaired tetralogy of Fallot (TOF) for long-term complications. Current risk assessment is based on volumetric and functional parameters that measure late expression of underlying physiological changes. Emerging 4-D flow MRI techniques promise new insights.

Objective—To assess whether 4-D flow MRI-derived measures of blood kinetic energy (1) differentiate children and young adults with TOF from controls and (2) are associated with disease severity.

Materials and methods—Pediatric patients post TOF repair (n=21) and controls (n=24) underwent 4-D flow MRI for assessment of time-resolved 3-D blood flow. Data analysis included 3-D segmentation of the right ventricle (RV) and pulmonary artery (PA), with calculation of peak systolic and diastolic kinetic energy (KE) maps. Total KE_{RV} and KE_{PA} were determined from the sum of the KE of all voxels within the respective time-resolved segmentations.

Results—KE_{PA} was increased in children post TOF vs. controls across the cardiac cycle, with median 12.5 (interquartile range [IQR] 10.3) mJ/m^2 vs. 8.2 (4.3) mJ/m^2, P<0.01 in systole; and 2.3 (2.7) mJ/m^2 vs. 1.4 (0.9) mJ/m^2, P<0.01 in diastole. Diastolic KE_{PA} correlated with systolic KE_{PA}

Correspondence to: Joshua D. Robinson.

Conflicts of interest None

(R^2 0.41, P<0.01) and with pulmonary regurgitation fraction (R^2 0.65, P<0.01). Diastolic KE_{RV} showed similar relationships, denoting increasing KE with higher cardiac outputs and increased right heart volume loading. Diastolic KE_{RV} and KE_{PA} increased with RV end-diastolic volume in a non-linear relationship (R^2 0.33, P<0.01 and R^2 0.50, P<0.01 respectively), with an inflection point near 120 mL/m^2.

Conclusion—Four-dimensional flow-derived KE is abnormal in pediatric patients post TOF repair compared to controls and has a direct, non-linear relationship with traditional measures of disease progression. Future longitudinal studies are needed to evaluate utility for early outcome prediction in TOF.

Keywords

Children; Congenital heart disease; 4-D flow; Heart; Kinetic energy; Magnetic resonance imaging; Pulmonary artery; Right ventricle; Tetralogy of Fallot

Introduction

Tetralogy of Fallot (TOF) accounts for approximately 10% of congenital heart disease and is the most common cyanotic congenital heart defect [1]. Surgical techniques have improved survival such that children with TOF require frequent and long-term surveillance for common postoperative sequelae, including residual right ventricular (RV) outflow tract obstruction, pulmonary regurgitation, RV dilatation or hypertrophy, and right or left ventricular dysfunction [2]. These complications are readily identified by MRI and are associated with impaired functional status, heart failure, surgical reintervention, atrial and ventricular arrhythmias, and sudden death [3–8]. Outcome prediction, however, remains imprecise and based on morphologic and simplified functional parameters (e.g., indexed ventricular volumes, ejection fraction), which measure late expression of underlying physiological changes [9, 10]. For example, in the repaired TOF patient with chronic pulmonary regurgitation, pulmonary valve replacement can halt or reverse RV dilatation [3, 11–13], but the risk of arrhythmia and sudden death might not be avoided [14, 15]. Consequently, early and more sensitive markers of deteriorating hemodynamics are needed.

Emerging 4-D flow MRI techniques hold great promise in this domain [16–20]. Four-dimensional flow MRI provides comprehensive hemodynamic information, allowing for assessment of complex flow patterns such as helical or vortical flow, and quantification of higher-order fluid dynamic metrics such as pressure difference maps [21–23], turbulent kinetic energy [24] and viscous energy loss [25]. Published findings in TOF, however, remain largely descriptive characterizations of abnormal flow patterns [26, 27] or comparisons to traditional 2-D MR flow parameters [28]. More recently, 4-D flow MRI has been used to noninvasively derive kinetic energy (KE) maps for visualization and quantification of flow energetics in the RV of people with repaired TOF [29]. Similarly, echocardiographic contrast particle imaging velocimetry has been used to map ventricular planar KE dissipation in a comparable population [30]. As a measure of the energy expended to overcome blood flow inertia, KE might signal deteriorating hemodynamics via excessive multi-directional energy dissipation. In other words, KE is a means of quantifying inefficiencies in the energetic transfer of ventricular contraction to net systolic blood flow.

Such inefficiencies play an especially important role in the child with repaired TOF with a post-surgical outflow tract or conduit [31], but 4-D advanced hemodynamic parameters have not yet been related to conventional outcome predictors such as RV volume or ejection fraction.

In this case-control study we explored quantitative 4-D flow MRI measures of right heart flow energetics that might be alternative markers of hemodynamic efficiency in pediatric patients with repaired TOF. We hypothesized that 4-D flow MRI-derived energetic biomarkers (1) can differentiate those with repaired TOF from healthy controls and (2) are associated with disease severity as measured by conventional clinical MRI parameters.

Materials and methods

We performed a single-center retrospective case-control study comparing pediatric and young adult patients with repaired TOF with an age-appropriate control population. All patients and control subjects underwent 4-D flow MRI immediately following a clinically indicated cardiovascular MRI exam between October 2011 and January 2016. Informed consent was obtained for performing 4-D flow per our prospective protocol. The protocol was approved by our institutional review board and complied with the Health Insurance Portability and Accountability Act.

We included children and young adults with TOF who had undergone staged or primary complete surgical correction before 3 years of age. We excluded patients with associated complex congenital heart disease (e.g., pulmonary atresia with major aortopulmonary collaterals, complete atrioventricular canal, or anomalous pulmonary venous drainage) or residual ventricular septal defect. The control population included patients ≤18 years of age with normal intracardiac structure and ventricular function, and no history of cardiothoracic surgery.

We identified 21 people with TOF who met study criteria and 24 control subjects who underwent MRI for evaluation of possible coronary anomaly (n=12), family history of sudden death or cardiomyopathy (n=7), possible bicuspid aortic valve (n=1) or extracardiac vascular anatomy (n=4). We collected baseline demographic data for all patients. We abstracted surgical description and clinical follow-up duration from operative reports and the electronic health record.

Magnetic resonance imaging

Imaging was performed on a 1.5-tesla (T) scanner (MAGNETOM Avanto or Aera; Siemens Healthcare USA, Malvern, PA). A 12-channel matrix coil was used for imaging on the Avanto and an 18-channel matrix coil on the Aera. Standard balanced steady-state free precession cine imaging, MR angiography and 2-D phase-contrast scans were obtained per routine clinical protocol and as appropriate for the assessment of patients with TOF [32]. MR angiography, 2-D phase-contrast MRI and 4-D flow were acquired following blood-pool contrast administration of 0.12 mL/kg gadofosveset trisodium (Ablavar; Lantheus Medical Imaging, North Billerica, MA) in all patients. Four-dimensional flow scan characteristics for this cohort were: spatial resolution = 1.4–4.5 × 1.1–3.1 × 1.4–3.5 mm^3, temporal resolution

= 36.0–44.8 ms, repetition time/echo time [TR/TE] = 4.7–5.1/2.2–3.0 ms, flip angle = 15°, and velocity sensitivity (VENC) = 100–250 cm/s. General anesthesia was administered by a pediatric anesthesiologist per the institutional clinical protocol for 10/21 (48%) people with TOF and 4/24 (17%) controls.

Image post-processing and 4-D data analysis

We measured ventricular volumes and function by conventional cine post-processing techniques [33] and standard clinical flow measurements derived from 2-D phase-contrast images using Medis QMass and QFlow (Leiden, The Netherlands), respectively. A single observer (M. J.R., a research assistant with 3 years of experience and a biomedical engineering background) corrected 4-D flow MRI data for velocity aliasing, Maxwell terms and eddy currents [34, 35], from which time-averaged 3-D phase-contrast MR angiograms were calculated. We then used commercial software (EnSight; CEI Software, Apex, NC) to determine the peak systolic (maximum PA outflow velocity) and peak diastolic (maximum tricuspid inflow, or E wave velocity) time points, or phases, from the pulmonary outflow and tricuspid valve inflow profiles, respectively (Fig. 1). We used another commercial application (Mimics; Materialise, Leuven, Belgium) to generate 3-D segmentation volumes of the main and proximal branch pulmonary arteries (PA) and right ventricle (RV) at peak systole and peak diastole (Fig. 1). A custom software tool developed in MATLAB (MathWorks, Natick, MA) was used to derive energetic parameters from RV and PA velocity masks similar to previously reported strategies used by Jeong et al. [29]. For each voxel inside the segmentation volumes, we calculated kinetic energy (KE). We calculated KE for a voxel of blood using the equation $KE = 1/2\ mv^2$, where mass (m) is voxel volume multiplied by density of blood (1.05 g/mL) and absolute velocity (v) is determined from 4-D flow data. We determined KE_{RV} and KE_{PA} from the sum of the KE of all voxels within the respective blood-pool segmentation, and calculated them for two phases (peak systole and peak diastole) in order to compare changes across the cardiac cycle. We generated KE maps for each phase by projecting mean KE on a 2-D plane transecting the RV and PA, respectively (Fig. 1). To normalize for patient and ventricular/vascular size, we indexed total KE values to body surface area (BSA) as well as segmentation volume of the PA and RV (in mL).

Statistical analysis

All continuous values are reported as median values with interquartile ranges. Patient characteristics, conventional MRI measurements and 4-D energetic biomarkers were not normally distributed and we applied the Mann-Whitney *U* test for comparison between groups. Differences were considered significant for $P<0.05$. To identify relationships between energetic biomarkers and conventional MRI parameters, we performed linear and polynomial regression analysis and calculated the correlation coefficient R^2; a correlation was considered significant for $P<0.05$. All statistical analysis was performed using MATLAB (MathWorks, Natick, MA) and SPSS (IBM, Armonk, NY).

Results

Patient demographics are summarized in Table 1. Age and gender distribution and body surface area were similar between people with TOF and controls, though those with TOF

had significant pulmonary regurgitation, increased ventricular size and diminished ventricular function, as expected. Three people with TOF had undergone RV–PA conduit placement as part of complete repair, two for near pulmonary atresia/severe pulmonary valve dysplasia and one because a conus coronary artery crossed the RV outflow tract. No one underwent pulmonary artery stent placement. Mean main PA velocity was 1.65±0.68 m/s.

Flow energetics — people with repaired tetrology of Fallot vs. healthy controls

There were significant differences in calculated right heart 4-D energetic parameters (Table 1). Kinetic energy was indexed to both patient size (body surface area in m^2) and the anatomically segmented volume (size of RV or PA in mL). KE_{PA} index was increased in people with TOF during systole (12.5 [IQR 10.3] vs. 8.2 [4.3] mJ/m^2, $P<0.01$; 0.19 [IQR 0.16] vs. 0.14 [IQR 0.07] mJ/mL, $P<0.01$) and during diastole (2.3 [IQR 2.7] vs. 1.4 [0.9] mJ/m^2, $P<0.01$; 0.034 [IQR 0.055] vs. 0.022 [IQR 0.009] mJ/mL, $P<0.01$). Diastolic KE_{RV} was greater in TOF than in controls only when indexed for ventricular size (0.034 [IQR 0.013] vs. 0.024 [0.012] mJ/mL, $P=0.02$). Figure 2 illustrates these differences, demonstrating the distribution of KE_{RV} and KE_{PA} across the cardiac cycle in a control subject and two people with TOF. Greater KE_{PA} was expended during systole in both people with TOF compared to the control patient, while KE_{RV} and KE_{PA} during diastole were increased only in the man with TOF with severe pulmonary regurgitation and right ventricular dilatation.

Flow energetics — relationships with ventricular performance and disease severity

Across patients and controls, systolic KE_{RV} and KE_{PA} significantly correlated with RV stroke volume ($R^2=0.58$, $P=0.0001$ and $R^2=0.61$, $P=0.0001$), denoting increasing kinetic energy at higher cardiac outputs. Similarly, there were strong relationships between diastolic and systolic KE_{RV} and KE_{PA} (R^2 0.38, $P<0.01$ and R^2 0.41, $P<0.01$, respectively; Fig. 3), further indicating that increased diastolic KE elicits higher systolic KE, or that the RV must compensate for pulmonary regurgitation with higher energy expenditures. In fact, in people with TOF, diastolic KE_{RV} and diastolic KE_{PA} were both significantly associated with degree of volume loading as assessed by pulmonary regurgitation fraction (R^2 0.54, $P<0.01$ and R^2 0.65, $P<0.01$ respectively; Fig. 3).

Most important, comparing indexed right ventricular end-diastolic volume (RVEDV) to diastolic KE_{RV} and KE_{PA} across both control and TOF populations demonstrated a non-linear relationship (R^2 0.33, $P<0.01$ and R^2 0.50, $P<0.01$, respectively). Figure 4 illustrates that at normal and smaller RV volumes, both control and TOF patients had relatively low KE_{RV} and KE_{PA} during diastole. As ventricular size increased beyond 120–130 mL/m^2, KE increased more rapidly and was best approximated by a second-order polynomial (R^2 0.50 and R^2 0.33, $P<0.01$).

Discussion

In the child with TOF with chronic pulmonary regurgitation, significant controversy remains regarding optimal timing of pulmonary valve replacement, with respect to both post-intervention RV remodeling and, more important, avoidance of major adverse outcomes

such as arrhythmias and sudden cardiac death. Risk assessments are based largely on morphologic and simplified functional parameters obtained from MRI but reflect late disease manifestations. Four-dimensional flow MRI offers whole-heart post-hoc calculation of traditional measures such as pulmonary regurgitation fraction, but also provides novel quantitative metrics to assess disease severity. In fact, our study demonstrates that measures of flow energetics derived from 4-D flow MRI, such as KE, are abnormal in children with TOF as compared to healthy controls and, more important, have a direct relationship with traditional measures of TOF disease severity such as RV size and pulmonary regurgitation fraction.

These observations confirm and build on prior work. Jeong et al. [29] measured time-resolved KE by 4-D flow MRI in the right and left ventricles of 10 subjects with TOF and demonstrated important differences compared to controls. While KE_{RV} and KE_{LV} did not have significant relationships with more conventional MRI outcome predictors, the number of subjects and the absolute differences in ventricular KE between subjects and controls were smaller than what we have observed in a larger cohort, and in both the RV and main and branch PAs. The authors noted that while absolute KE_{RV} and KE_{LV} were higher in people with TOF, forward flow in the PA and aorta were similar compared to controls, indicating greater kinetic energy in the RV and LV without increased pulmonary or systemic flow and implying ventricular–vascular inefficiency. Indeed, the higher degree of kinetic energy that we observed in the downstream vasculature supports such an assumption, and the direct and non-linear relationship of these energetic biomarkers with routine measurements of ventricular performance (e.g., RVEDV, stroke volume) suggests that they might be earlier predictors of disease progression. In fact, the strong relationship that we observed between diastolic and systolic KE is further indication that increased diastolic energy triggers higher systolic flow energy, or that chronic pulmonary regurgitation directly increases myocardial workload in a measurable fashion. Moreover, the dramatic increase noted in KE_{PA} with more severe RV enlargement is evidence of impaired ventricular–vascular coupling and a compelling argument that these inefficiencies precede changes such as ventricular remodeling and decreased performance.

Interestingly, Fogel and colleagues [31] assessed 13 patients with TOF by a combination of cardiac MRI and invasive hemodynamic catheterization to estimate RV power output and energy loss in patients with chronic pulmonary regurgitation. The authors found a strong negative correlation between RV power output and normalized ventricular volumes, with an exponential decrease in power output beyond right ventricular end-diastolic volume (RVEDV) of 120–140 mL/m^2 and right ventricular end-systolic volume (RVESV) of 65–75 mL/m^2. These inflection points are similar to the trend we demonstrated between KE of the right heart and increasing RV size in our TOF cohort. It is important to note, however, that our estimation of flow energy (KE_{PA}) was derived entirely from 4-D flow MRI and in a noninvasive fashion and might be a more practical and low-risk means of assessing evolving hemodynamic inefficiency.

Noninvasively derived 4-D energetic biomarkers of RV efficiency could directly influence indications for reintervention in TOF. Current indications for pulmonary valve replacement are based on pulmonary regurgitation fraction, RV volumes, biventricular ejection fraction

and exercise intolerance, with significant weight given to an indexed RVEDV threshold of 150–170 mL/m^2 While the optimal volumetric threshold is controversial [36, 37], multiple studies have generated more enthusiasm for early intervention at smaller ventricular sizes [15, 38–40]. In a retrospective MRI study of adults with TOF before and after pulmonary valve replacement, indexed RVEDV and RVESV decreased 34% and 37%, respectively, and no patients with an RVEDV >170 mL/m^2 or RVESV >85 mL/m^2 before pulmonary valve replacement had “normalization” of RV volumes after surgery [40]. In another single-center prospective study, Buechel and colleagues [39] performed MRI on people with TOF following pulmonary valve replacement using a threshold RVEDV of 150 mL/m^2 and demonstrated prompt RV remodeling, with substantial reduction of RV volume and mass at 6 months after surgery. It is important to note that none of the referenced studies discerned a volumetric threshold that reliably predicts postoperative course free of arrhythmia or sudden death. Longitudinal comparison of other markers such as KE with these major adverse events and other clinical endpoints such as functional capacity is needed.

Several studies have evaluated routine parameters of ventricular function or flow to predict the postoperative outcomes in people with TOF and chronic pulmonary regurgitation. Although standard MRI parameters are the best available predictors of functional status, they do not correlate directly with decreasing exercise capacity [41], a common finding in repaired TOF [42–47], and not unexpected given the greatly increased hemodynamic demands imposed on the RV during exercise. Past studies have implicated numerous factors in this impairment, including pulmonary regurgitation, PA distortion, impaired lung function, chronotropic impairment, and ventricular dysfunction [42–47], but energetic markers might be earlier and more comprehensive markers of the hemodynamic inefficiencies that drive exercise intolerance. Kinetic energy, for example, represents a small percentage (1–6%) of total ventricular work at rest but plays a substantially larger role during activity [48]. Unfortunately, our study was retrospective in nature and the available exercise data were insufficient to draw any meaningful conclusions about these relationships. Further study, including exercise or pharmacological stress MRI, is needed to assess whether the small changes in KE at rest signal inefficiencies that are more dramatic during exercise and more closely correlate with exercise capacity than traditional parameters.

Our retrospective study is limited by its small sample size, the heterogeneity of patients with TOF and a limited pediatric control population. We also included people who received a gadolinium-based blood-pool contrast agent that is no longer commercially available. Inclusion of both fully conscious and anesthetized patients also introduces some heterogeneity in the TOF patient population, but this limitation is inherent to the retrospective design and reflects real-world variability. While our study would be strengthened by age- and BSA-matched controls, clinical indications for cardiac MRI in a young cohort are very narrow and volunteer recruitment is unfeasible. A lack of a reference or gold standard for flow energetic measures is another limitation. It is important to note that we analyzed KE maps only at peak systolic and diastolic timepoints, though information is available across the entire cardiac cycle. This is a limitation in our workflow but future studies and analysis tools could incorporate this information. Finally, in some patients with pulmonary stenosis, VENC settings might have limited dynamic range, which is particularly

important in discriminating the lower velocities observed in the RV and great arteries during diastole. Nonetheless, we did observe significant differences in diastolic energetic markers.

Conclusion

Over the decades following TOF repair, the increased energy demands associated with chronic pulmonary regurgitation contribute to excess myocardial work and can lead to untimely heart failure and other life-threatening complications. Four-dimensional flow MRI energetic measures, such as kinetic energy, are abnormal in repaired TOF compared to controls, have a direct and non-linear relationship with traditional measures of disease severity, and might be an earlier predictor of evolving hemodynamic inefficiency than traditional parameters. Longitudinal observation is needed to assess the utility of MRI flow energetics for predicting impaired ventricular–vascular coupling relationships and deteriorating hemodynamics. Comparison to exercise capacity and clinical outcomes in a larger cohort is warranted.

Acknowledgments

This work was supported by the National Heart, Lung, and Blood Institute at the National Institutes of Health [R01HL115828 and K25HL119608].

References

1. Talner CN (1998) Report of the New England Regional Infant Cardiac Program, by Donald C. Fyler, MD, Pediatrics, 1980;65(suppl):375–461. Pediatrics 102:258–259 [PubMed: 9651450]
2. Valente AM, Cook S, Festa P et al. (2014) Multimodality imaging guidelines for patients with repaired tetralogy of Fallot: a report from the American Society of Echocardiography: developed in collaboration with the Society for Cardiovascular Magnetic Resonance and the Society for Pediatric Radiology. J Am Soc Echocardiogr 27:111–141 [PubMed: 24468055]
3. Geva T (2006) Indications and timing of pulmonary valve replacement after tetralogy of Fallot repair. Semin Thorac Cardiovasc Surg Pediatr Card Surg Annu 2006:11–22
4. Bacha EA, Scheule AM, Zurakowski D et al. (2001) Long-term results after early primary repair of tetralogy of Fallot. J Thorac Cardiovasc Surg 122:154–161 [PubMed: 11436049]
5. Nollert G, Fischlein T, Bouterwek S et al. (1997) Long-term survival in patients with repair of tetralogy of Fallot: 36-year follow-up of 490 survivors of the first year after surgical repair. J Am Coll Cardiol 30:1374–1383 [PubMed: 9350942]
6. Gatzoulis MA, Balaji S, Webber SA et al. (2000) Risk factors for arrhythmia and sudden cardiac death late after repair of tetralogy of Fallot: a multicentre study. Lancet 356:975–981 [PubMed: 11041398]
7. Hickey EJ, Veldtman G, Bradley TJ et al. (2012) Functional health status in adult survivors of operative repair of tetralogy of Fallot. Am J Cardiol 109:873–880 [PubMed: 22244382]
8. Kaza AK, Lim HG, Dibardino DJ et al. (2009) Long-term results of right ventricular outflow tract reconstruction in neonatal cardiac surgery: options and outcomes. J Thorac Cardiovasc Surg 138:911–916 [PubMed: 19660342]
9. Knauth AL, Gauvreau K, Powell AJ et al. (2008) Ventricular size and function assessed by cardiac MRI predict major adverse clinical outcomes late after tetralogy of Fallot repair. Heart 94:211–216 [PubMed: 17135219]
10. Valente AM, Gauvreau K, Assenza GE et al. (2014) Contemporary predictors of death and sustained ventricular tachycardia in patients with repaired tetralogy of Fallot enrolled in the INDICATOR cohort. Heart 100:247–253 [PubMed: 24179163]

11. Tweddell JS, Simpson P, Li SH et al. (2012) Timing and technique of pulmonary valve replacement in the patient with tetralogy of Fallot. Semin Thorac Cardiovasc Surg Pediatr Card Surg Annu 15:27–33 [PubMed: 22424505]
12. Frigiola A, Hughes M, Turner M et al. (2013) Physiological and phenotypic characteristics of late survivors of tetralogy of Fallot repair who are free from pulmonary valve replacement. Circulation 128:1861–1868 [PubMed: 24065608]
13. Geva T (2013) Indications for pulmonary valve replacement in repaired tetralogy of Fallot: the quest continues. Circulation 128:1855–1857 [PubMed: 24065609]
14. Harrild DM, Berul CI, Cecchin F et al. (2009) Pulmonary valve replacement in tetralogy of Fallot: impact on survival and ventricular tachycardia. Circulation 119:445–451 [PubMed: 19139389]
15. Oosterhof T, van Straten A, Vliegen HW et al. (2007) Preoperative thresholds for pulmonary valve replacement in patients with corrected tetralogy of Fallot using cardiovascular magnetic resonance. Circulation 116:545–551 [PubMed: 17620511]
16. Dyverfeldt P, Bissell M, Barker AJ et al. (2015) 4D flow cardiovascular magnetic resonance consensus statement. J Cardiovasc Magn Reson 17:72 [PubMed: 26257141]
17. Markl M, Frydrychowicz A, Kozerke S et al. (2012) 4D flow MRI. J Magn Reson Imaging 36:1015–1036 [PubMed: 23090914]
18. Frydrychowicz A, Francois CJ, Turski PA (2011) Four-dimensional phase contrast magnetic resonance angiography: potential clinical applications. Eur J Radiol 80:24–35 [PubMed: 21333479]
19. Hope MD, Sedlic T, Dyverfeldt P (2013) Cardiothoracic magnetic resonance flow imaging. J Thorac Imaging 28:217–230 [PubMed: 23708687]
20. Roldan-Alzate A, Francois CJ, Wieben O et al. (2016) Emerging applications of abdominal 4D flow MRI. AJR Am J Roentgenol 207:58–66 [PubMed: 27187681]
21. Bock J, Frydrychowicz A, Lorenz R et al. (2011) In vivo noninvasive 4D pressure difference mapping in the human aorta: phantom comparison and application in healthy volunteers and patients. Magn Reson Med 66:1079–1088 [PubMed: 21437978]
22. Ebbers T, Wigstrom L, Bolger AF et al. (2002) Noninvasive measurement of time-varying three-dimensional relative pressure fields within the human heart. J Biomech Eng 124:288–293 [PubMed: 12071263]
23. Tyszka JM, Laidlaw DH, Asa JW et al. (2000) Three-dimensional, time-resolved (4D) relative pressure mapping using magnetic resonance imaging. J Magn Reson Imaging 12:321–329 [PubMed: 10931596]
24. Dyverfeldt P, Hope MD, Tseng EE et al. (2013) Magnetic resonance measurement of turbulent kinetic energy for the estimation of irreversible pressure loss in aortic stenosis. JACC Cardiovasc Imaging 6:64–71 [PubMed: 23328563]
25. Barker AJ, van Ooij P, Bandi K et al. (2014) Viscous energy loss in the presence of abnormal aortic flow. Magn Reson Med 72:620–628 [PubMed: 24122967]
26. Geiger J, Markl M, Jung B et al. (2011) 4D-MR flow analysis in patients after repair for tetralogy of Fallot. Eur Radiol 21:1651–1657 [PubMed: 21720942]
27. Francois CJ, Srinivasan S, Schiebler ML et al. (2012) 4D cardiovascular magnetic resonance velocity mapping of alterations of right heart flow patterns and main pulmonary artery hemodynamics in tetralogy of Fallot. J Cardiovasc Magn Reson 14:16 [PubMed: 22313680]
28. Gabbour M, Schnell S, Jarvis K et al. (2015) 4-D flow magnetic resonance imaging: blood flow quantification compared to 2-D phase-contrast magnetic resonance imaging and Doppler echocardiography. Pediatr Radiol 45:804–813 [PubMed: 25487721]
29. Jeong D, Anagnostopoulos PV, Roldan-Alzate A et al. (2015) Ventricular kinetic energy may provide a novel noninvasive way to assess ventricular performance in patients with repaired tetralogy of Fallot. J Thorac Cardiovasc Surg 149:1339–1347 [PubMed: 25623907]
30. Kutty S, Li L, Danford DA et al. (2014) Effects of right ventricular hemodynamic burden on intraventricular flow in tetralogy of Fallot: an echocardiographic contrast particle imaging velocimetry study. J Am Soc Echocardiogr 27:1311–1318 [PubMed: 25450015]

31. Fogel MA, Sundareswaran KS, de Zelicourt D et al. (2012) Power loss and right ventricular efficiency in patients after tetralogy of Fallot repair with pulmonary insufficiency: clinical implications. J Thorac Cardiovasc Surg 143:1279–1285 [PubMed: 22154796]
32. Fratz S, Chung T, Greil GF et al. (2013) Guidelines and protocols for cardiovascular magnetic resonance in children and adults with congenital heart disease: SCMR expert consensus group on congenital heart disease. J Cardiovasc Magn Reson 15:51 [PubMed: 23763839]
33. Alfakih K, Plein S, Thiele H et al. (2003) Normal human left and right ventricular dimensions for MRI as assessed by turbo gradient echo and steady-state free precession imaging sequences. J Magn Reson Imaging 17:323–329 [PubMed: 12594722]
34. Bernstein MA, Zhou XJ, Polzin JA et al. (1998) Concomitant gradient terms in phase contrast MR: analysis and correction. Magn Reson Med 39:300–308 [PubMed: 9469714]
35. Walker PG, Cranney GB, Scheidegger MB et al. (1993) Semiautomated method for noise reduction and background phase error correction in MR phase velocity data. J Magn Reson Imaging 3:521–530 [PubMed: 8324312]
36. O'Byrne ML, Glatz AC, Mercer-Rosa L et al. (2015) Trends in pulmonary valve replacement in children and adults with tetralogy of Fallot. Am J Cardiol 115:118–124 [PubMed: 25456860]
37. Holmes KW (2012) Timing of pulmonary valve replacement in tetralogy of Fallot using cardiac magnetic resonance imaging: an evolving process. J Am Coll Cardiol 60:1015–1017 [PubMed: 22921970]
38. Lee C, Kim YM, Lee CH et al. (2012) Outcomes of pulmonary valve replacement in 170 patients with chronic pulmonary regurgitation after relief of right ventricular outflow tract obstruction: implications for optimal timing of pulmonary valve replacement. J Am Coll Cardiol 60:1005–1014 [PubMed: 22921969]
39. Buechel ER, Dave HH, Kellenberger CJ et al. (2005) Remodelling of the right ventricle after early pulmonary valve replacement in children with repaired tetralogy of Fallot: assessment by cardiovascular magnetic resonance. Eur Heart J 26:2721–2727 [PubMed: 16214832]
40. Therrien J, Provost Y, Merchant N et al. (2005) Optimal timing for pulmonary valve replacement in adults after tetralogy of Fallot repair. Am J Cardiol 95:779–782 [PubMed: 15757612]
41. Kipps AK, Graham DA, Harrild DM et al. (2011) Longitudinal exercise capacity of patients with repaired tetralogy of fallot. Am J Cardiol 108:99–105 [PubMed: 21529748]
42. Fredriksen PM, Therrien J, Veldtman G et al. (2002) Aerobic capacity in adults with tetralogy of Fallot. Cardiol Young 12:554–559 [PubMed: 12636004]
43. Mahle WT, McBride MG, Paridon SM (2002) Exercise performance in tetralogy of Fallot: the impact of primary complete repair in infancy. Pediatr Cardiol 23:224–229 [PubMed: 11889543]
44. Rowe SA, Zahka KG, Manolio TA et al. (1991) Lung function and pulmonary regurgitation limit exercise capacity in postoperative tetralogy of Fallot. J Am Coll Cardiol 17:461–466 [PubMed: 1991905]
45. Sutton NJ, Peng L, Lock JE et al. (2008) Effect of pulmonary artery angioplasty on exercise function after repair of tetralogy of Fallot. Am Heart J 155:182–186 [PubMed: 18082511]
46. Wessel HU, Cunningham WJ, Paul MH et al. (1980) Exercise performance in tetralogy of Fallot after intracardiac repair. J Thorac Cardiovasc Surg 80:582–593 [PubMed: 7421291]
47. Gatzoulis MA, Clark AL, Cullen S et al. (1995) Right ventricular diastolic function 15 to 35 years after repair of tetralogy of Fallot. Restrictive physiology predicts superior exercise performance. Circulation 91:1775–1781 [PubMed: 7882487]
48. Prec O, Katz LN (1949) Determination of kinetic energy of the heart in man. Am J Physiol 159:483–491 [PubMed: 15401092]

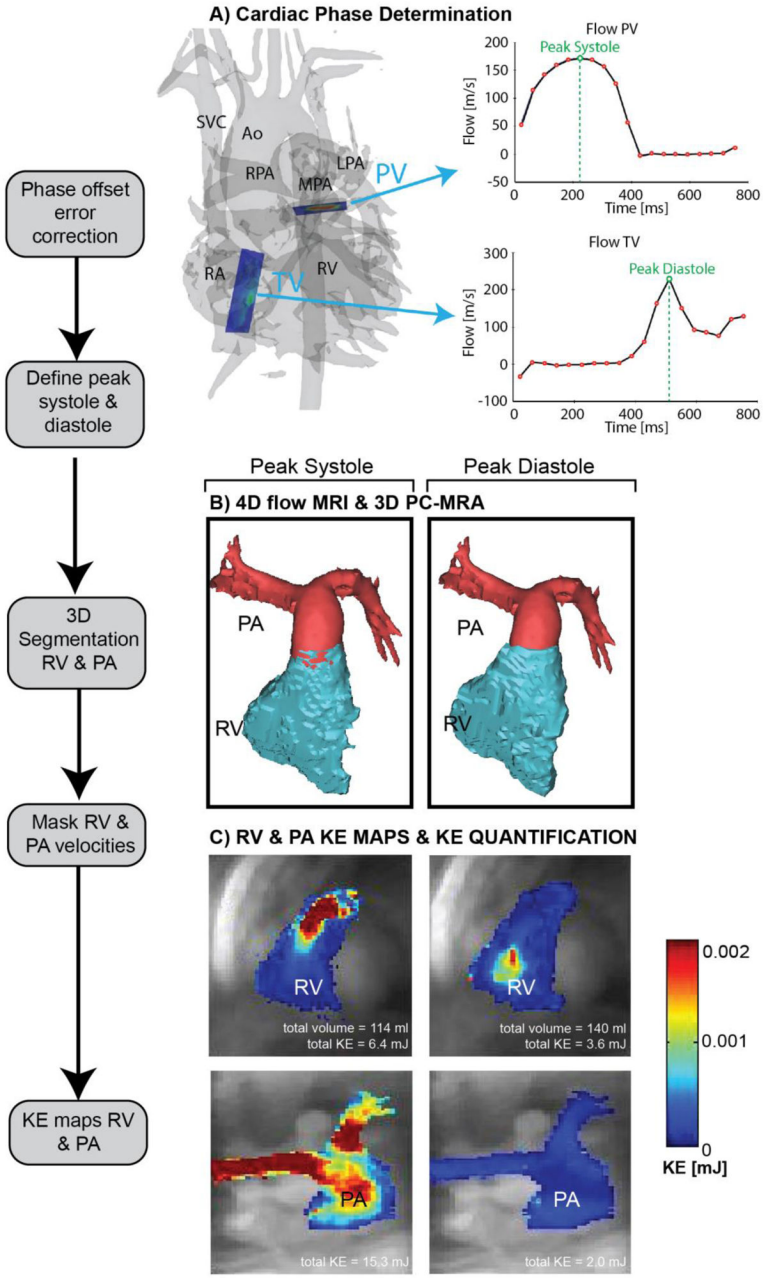

Fig. 1.

Four-dimensional (4-D) flow MRI data analysis. **a** Four-dimensional flow-derived 3-D phase-contrast MR angiogram and 2-D analysis planes at the level of the pulmonary valve (PV) and tricuspid valve (TV). The analysis planes were used to calculate flow–time curves to determine peak systole and diastole via peak flow rates. **b** Three-dimensional segmentations of the right ventricle (RV) and pulmonary artery (PA) based on the 3-D phase-contrast MR angiography data and masking of velocities inside the segmented vessels. Separate segmentations were generated for peak systole and peak diastol. **c** Calculation of RV and PA kinetic energy (KE) maps during systole and diastole. Total KE is listed below

each map. *Ao* aorta, *LPA* left pulmonary artery, *MPA* main pulmonary artery, *RA* right atrium, *RPA* right pulmonary artery, *SVC* superior vena cava

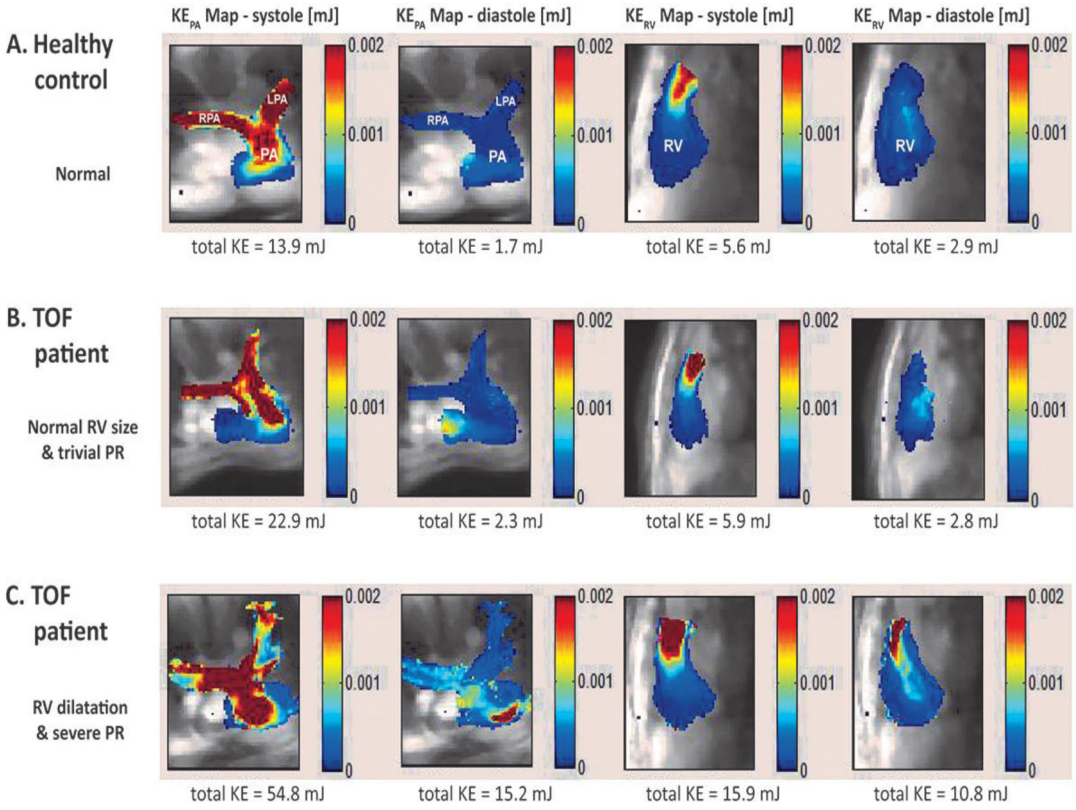

Fig. 2.

Maps of kinetic energy (KE) superimposed on the underlying anatomical 4-D flow MRI data. The individual images show KE maps during peak systole and peak diastole in three subjects (**a,** control; **b, c** people with tetralogy of Fallot). Color coding illustrates regions with high (*red*) and low (*blue*) kinetic energy. Note increased total KE in a 21-year-old man with TOF with right ventricular dilatation and severe pulmonary regurgitation (**c**, compared to a 16-year-old male control (**a**) and a 15-year-old girl with TOF with normal right ventricular size and trivial pulmonary regurgitation (**b**). *LPA* left pulmonary artery, *PA* pulmonary artery, *PR* pulmonary regurgitation, *RPA* right pulmonary artery, *RV* right ventricle

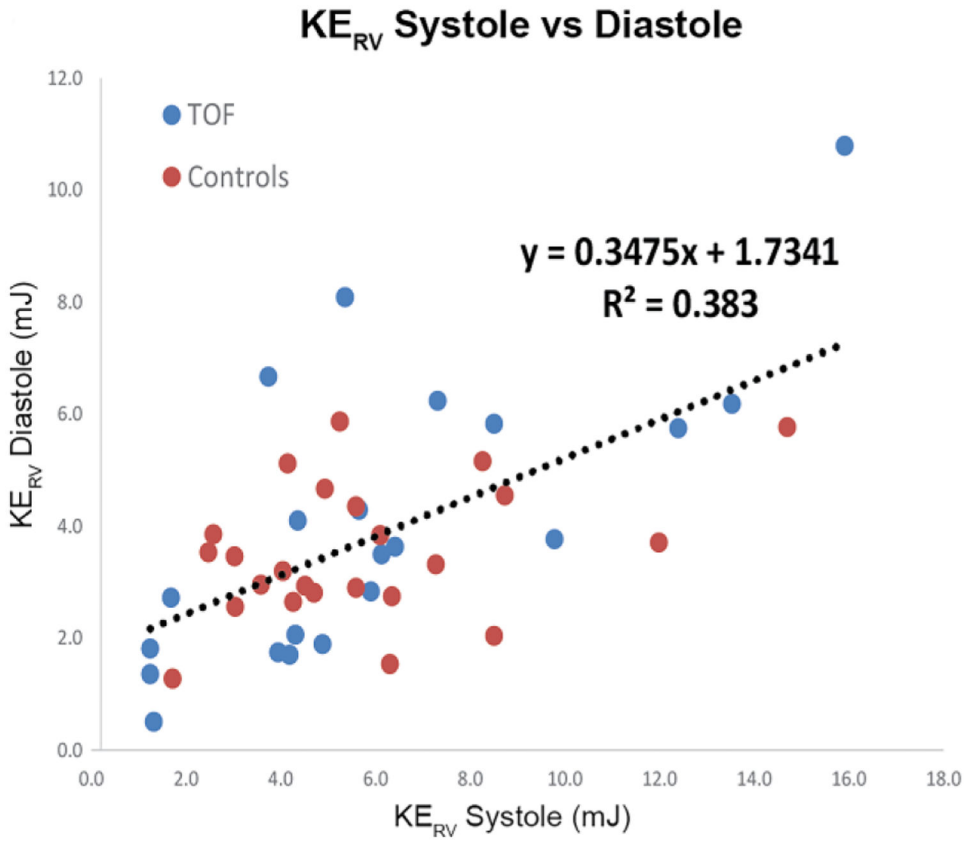

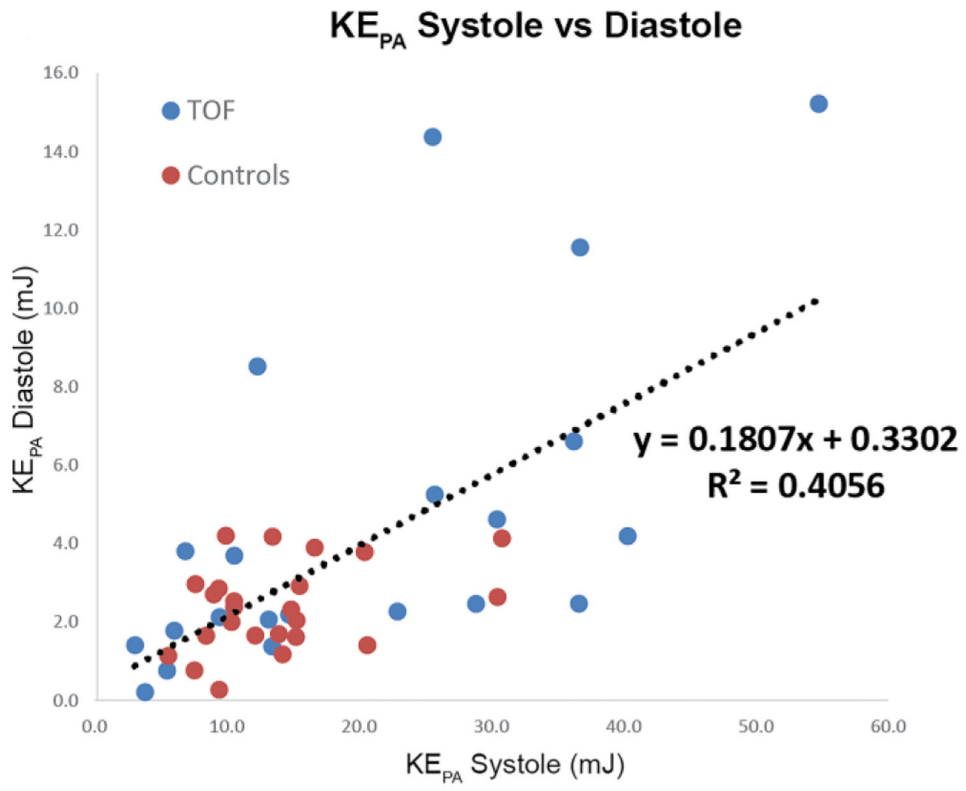

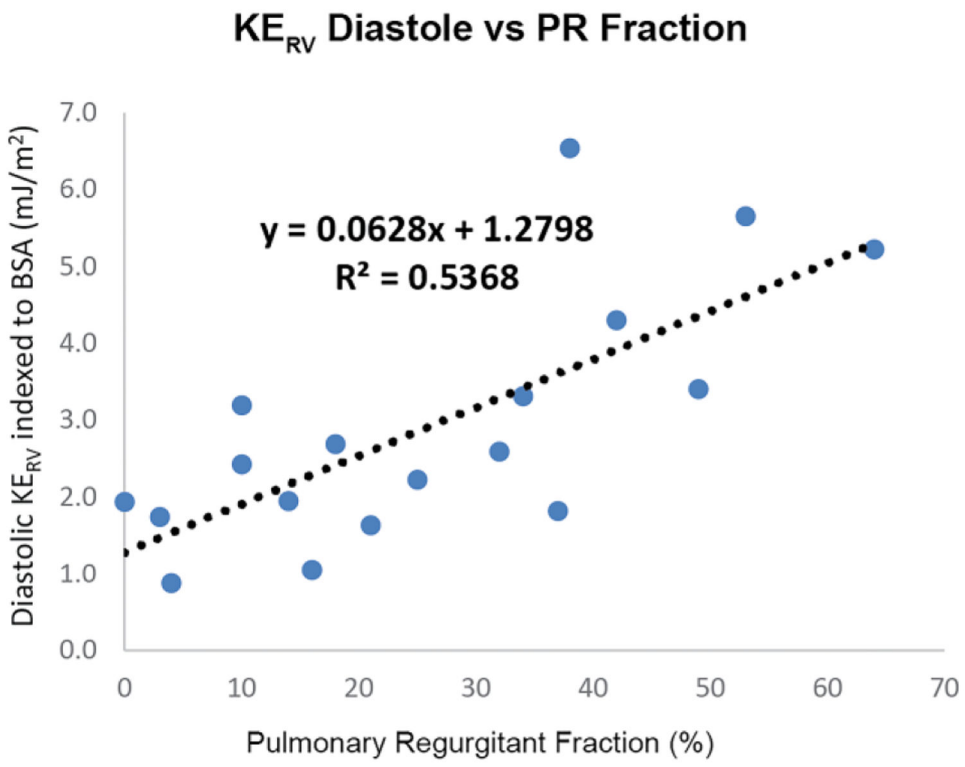

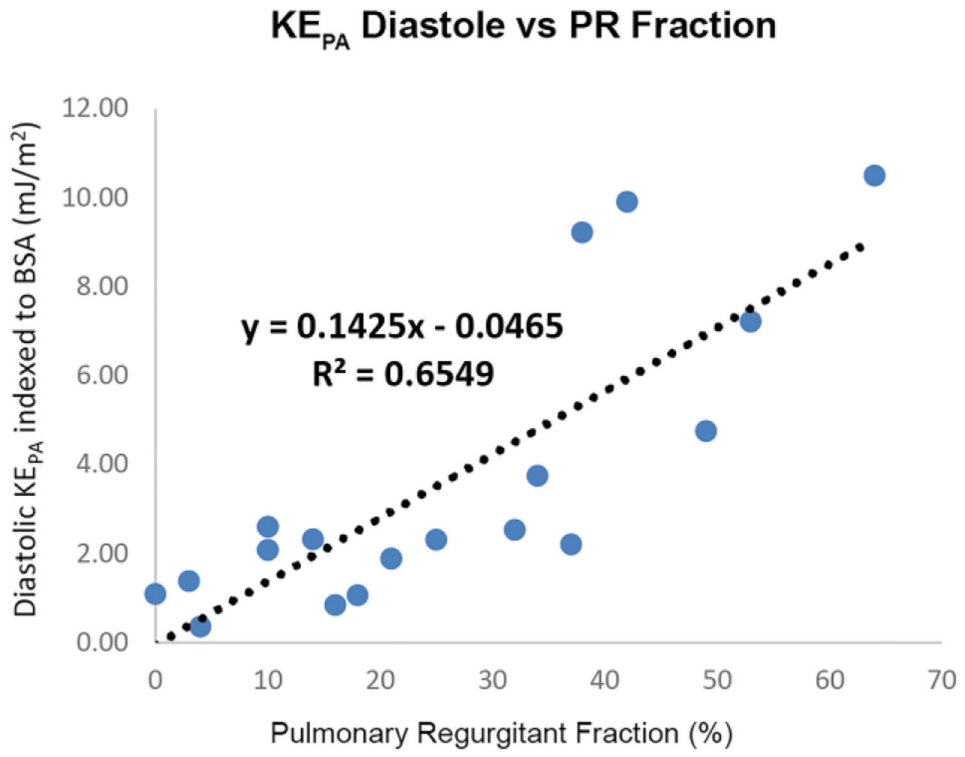

Fig. 3.

Right heart kinetic energy (KE) increases with cardiac output and degree of volume loading because of pulmonary regurgitation. **a, b** Increased diastolic KE is strongly associated with

increased systolic KE in both the right ventricle (RV) and pulmonary artery (PA), respectively. **c, d** Diastolic KE_{RV} and KE_{PA} are strongly related to pulmonary regurgitation fraction. *BSA* body surface area

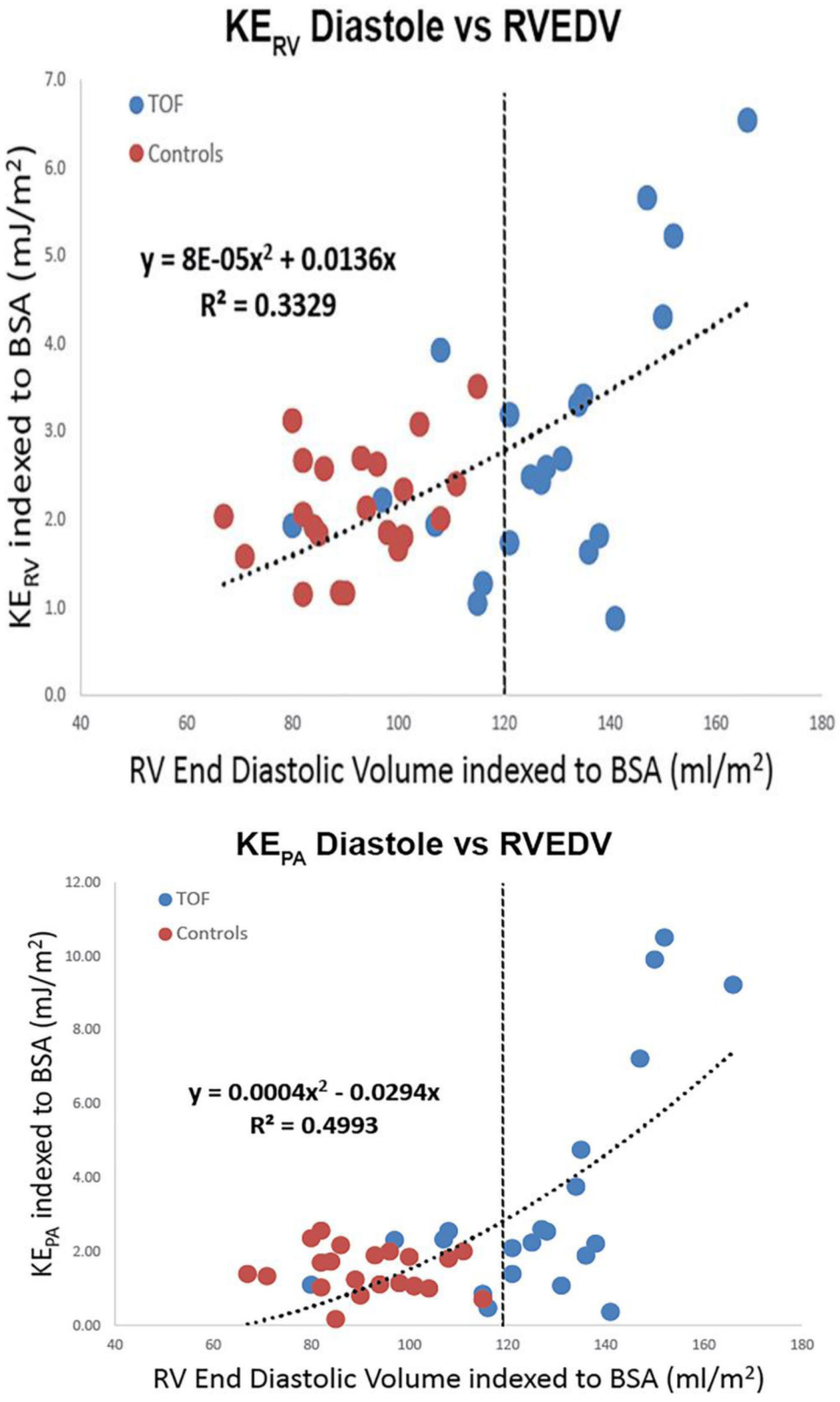

Fig. 4.

Right heart kinetic energy (KE) during diastole is associated with right ventricular (RV) size. When normalized to body surface area (BSA), both KE_{RV} (**a**) and KE_{PA} (**b**) demonstrate strong positive correlations with right ventricular end-diastolic volume (RVEDV) across both control patients and people with tetralogy of Fallot, with KE_{PA} increasing more rapidly beyond an inflection point of 120 mL/m^2 (*dashed lines*). *PA* pulmonary artery

Table 1

Patient and control cohort characteristics

	Post TOF repair[a] (*n*=21)	Controls[a] (*n*=24)	*P*-value[b]
Age	13.8 (8.2)	15.8 (3.0)	0.18
n (female)	13	13	N/A
Body surface area (m^2)	1.62 (0.70)	1.62 (0.28)	0.25
Standard MRI parameters			
PR fraction (%) by flow	23 (28)	N/A	N/A
PR fraction (%) by volumetry	19 (30)	0 (6.7)	<0.01
RVEDV index (mL/m^2)	128 (23)	92 (19)	<0.01
RVESV index (mL/m^2)	70 (13)	41 (11)	<0.01
RV stroke volume (mL)	88 (44)	76 (19)	0.81
RV ejection fraction (%)	47 (11)	56 (10)	<0.01
RVCI ($L/min/m^2$)	3.7 (2.2)	3.6 (0.8)	0.15
LVEDV index (mL/m^2)	91 (15)	87 (16)	0.27
LVESV index (mL/m^2)	41 (11)	35 (7)	<0.01
LV stroke volume (mL)	63 (50)	80 (20)	0.09
LV ejection fraction (%)	55 (9.5)	60 (6)	<0.01
LVCI ($L/min/m^2$)	3.3 (0.8)	3.7 (0.8)	0.05
Ratio pulmonary-to-aortic flow	0.95 (0.22)	N/A	N/A
4-D flow MRI energetic parameters,[c] absolute and indexed to body surface area and segmentation volume			
Systole			
KE_{RV} (mJ)	5.4 (3.7)	5.1 (3.0)	0.92
KE_{PA} (mJ)	14.7 (23)	12.8 (6.0)	0.27
KE_{RV} index (mJ/m^2)	3.4 (2.3)	3.3 (2.0)	0.5
KE_{PA} index (mJ/m^2)	12.5 (10.3)	8.2 (4.3)	<0.01
KE_{RV} index (mJ/mL)	0.056 (0.048)	0.047 (0.03)	0.12
KE_{PA} index (mJ/mL)	0.193 (0.16)	0.138 (0.072)	<0.01
Diastole			
KE_{RV} (mJ)	3.6 (4.0)	3.4 (1.7)	0.78
KE_{PA} (mJ)	2.5 (3.6)	2.4 (1.3)	0.13
KE_{RV} index (mJ/m^2)	2.5 (1.8)	2.1 (0.92)	0.18
KE_{PA} index (mJ/m^2)	2.3 (2.7)	1.4 (0.9)	<0.01
KE_{RV} index (mJ/ml)	0.034 (0.013)	0.024 (0.012)	0.02
KE_{PA} index (mJ/mL)	0.034 (0.055)	0.022 (0.009)	<0.01

[a] Standard MRI measurements and 4-D flow MRI-derived energetic calculations presented as median (interquartile range). Energetic markers are indexed to both body surface area (mJ/m^2) and segmentation volume (mJ/ml)

[b] Differences were considered significant for $P<0.05$

[c] Energetic parameters are reported in absolute (mJ) and normalized values, indexed to both body surface area (mJ/m^2) and segmentation volume (mJ/mL)

KE kinetic energy, *LV* left ventricle, *LVCI* left ventricle cardiac index, *LVEDV* left ventricle end-diastolic volume, *N/A* not available, *PA* pulmonary artery, *PR* pulmonary regurgitation, *RV* right ventricle, *RVCI* right ventricle cardiac index, *RVEDV* right ventricle end-diastolic volume, *LVESV* left ventricle end-systolic volume, *RVESV* right ventricle end-systolic volume, *TOF* tetralogy of Fallot